Journal of Catalysis **212,** 145–156 (2002)
doi:10.1006/jcat.2002.3783

Role of Synthesis Method and Particle Size of Nanostructured TiO_2 on Its Photoactivity

Catherine B. Almquist* and Pratim Biswas†,[1]

*Paper Science and Engineering Department, Miami University, Oxford, Ohio 45056; and †Environmental Engineering Science Program, Departments of Chemical and Civil Engineering, One Brookings Drive, Campus Box 1180, Washington University in St. Louis, St. Louis, Missouri 63130-4899

Received February, 13, 2002; revised July 30, 2002; accepted August 8, 2002

TiO_2 prepared by different methods was used to obtain anatase powders with particle sizes ranging from 5 to 165 nm. Powders were prepared using two methods: (i) a flame aerosol process in which nanoparticles of TiO_2 were synthesized in a flame on oxidation (combustion) of an organotitanium precursor, and (ii) calcination of commercially available nanostructured TiO_2 (Ishihara ST-01, 5 nm, as received). For comparison, Degussa P25 and Aldrich anatase TiO_2 powders were also used as received. The TiO_2 powders were characterized using XRD to determine crystal phase and crystal size, BET surface area analyses, *uv–vis* absorbtion spectroscopy to determine the band gap, and experiments in which the photoxidation rate of phenol in water was used as a measure of photoactivity. A model was developed based on the mechanistic steps in photocatalysis to elucidate the role of particle size on the apparent photoactivity of TiO_2 for the photooxidation of organic substrates in water. The model was used to explain the trends in the experimental data for four different sets of photoactivity experiments with TiO_2 powders. The results of this study elucidate a strong effect of particle size on photoactivity. The effects of particle size on the efficiency of light absorption and scattering and charge-carrier dynamics at particle sizes less than 25 nm dominate the apparent photoactivity of TiO_2, and an optimum particle size of 25 to 40 nm exists within all sets of photocatalysis experiments conducted with TiO_2 powders in this study. The optimum particle size is a result of competing effects of effective particle size on light absorption and scattering efficiency, charge-carrier dynamics, and surface area.

INTRODUCTION

Heterogeneous photocatalysis with titanium dioxide (TiO_2) has been extensively investigated as a method to oxidize organic pollutants in water and air. TiO_2 is the most widely used photocatalyst because it is a relatively safe and inexpensive semiconductor that is stable to photocorrosion. However, it has been found that the process and processing conditions under which the TiO_2 powders are synthesized lead to significant variations in their structure, particle size, stoichiometry, optical and electronic properties, and, hence, photoactivity (1, 2). TiO_2 has been synthesized in research laboratories by several methods, including flame oxidation and sol–gel processes. In flame oxidation processes, anatase and rutile TiO_2 particles of varying particle sizes are formed in the flame, depending on the flame conditions, and the resulting TiO_2 powders do not require subsequent calcination. In the sol–gel synthesis of TiO_2, nanoparticles are formed in a gel which are recovered on drying of the gel. However, sol–gel processing requires subsequent calcination to obtain crystals of anatase and rutile TiO_2 of varying particle sizes, depending on the time-temperature profile of the calcination procedure.

The effect of particle size on the photoactivity of TiO_2 was investigated by several researchers (3–8). Experimental investigations led to the discovery that an optimum particle size of TiO_2 exists such that the photocatalytic oxidation rates of organic substrates are maximized. Wang *et al.* (3) found that an optimum particle size of approximately 11 nm exists for the destruction of chloroform in water. The authors' concluded that the opposing effects of larger surface area but higher rate of electron–hole recombination at the particle surface as particle size decreases, due to the enhanced proximity of the charges, results in an optimum particle size. Maira *et al.* (5) found an optimum particle size of 7 nm for the gas-phase photooxidation of trichloroethylene. The authors concluded that the optimum particle size was observed due to the off-setting contributions of high surface area and changes in the structural and electronic properties of the TiO_2 as the particle size decreases in the nanometer scale.

Theoretical investigations, via mathematical models, have also concluded that particle size has a significant role in the photoactivity of TiO_2. Gerischer (6) developed a model based upon the mechanistic steps in photocatalysis on TiO_2, which predicts a significant increase in quantum yield (defined as the ratio of electron–hole pairs involved in redox reactions at the surface of the titanium dioxide particles to total electron–hole pairs generated) as particle size

[1] To whom correspondence should be addressed. E-mail: Pratim.Biswas@seas.wustl.edu.

0021-9517/02 $35.00

decreases from 1000 to 10 nm. Since the efficiency of light absorption decreases as particle size decreases in this range, fewer electron–hole pairs are generated. The predicated increase in quantum yield by Gerischer's model was a result of the model predicting a higher fraction of the electron–hole pairs partaking in redox reactions at the surface when fewer electron–hole pairs were generated within the particle. Grela and Colussi (7) developed a computer stochastic model that predicted an increase in quantum yield as particle size increased from 3 to 21 nm. The authors reasoned that quantum yield increased as particle size increased in this range because the electron–hole recombination rates at the surface were slower, which supports the hypothesis of Wang *et al.* (3). Slower electron–hole recombination in the Grela and Colussi (7) model as particle size increased to 21 nm was a result of at least two assumptions made in the model development: (i) the average initial distance between electron–hole pairs is proportional to the radius of the TiO_2 particle (R), and (ii) the average number of jumps before a free hole at the surface recombines with a trapped electron is proportional to R^2 (7). Neither model (6, 7) considered the effects of electron–hole recombination within the particle volume; it was assumed that diffusion of the electrons and holes to the surface of the particle was a relatively fast process in nanostructured TiO_2, and that they reach the surface before partaking in recombination reactions.

In this study, we compared the apparent photoactivities of flame-synthesized TiO_2 and commercially available TiO_2 as received and after calcination in air at temperatures ranging from 200 to 700°C. The TiO_2 powders had an overall range of effective particle sizes (based upon BET surface area) from approximately 5 to 165 nm. The photooxidation rate of phenol was used as a measure of photoactivity of TiO_2. The results were compared and discussed to illustrate the effect of crystal size and effective particle size on the apparent photoactivity of TiO_2 powders in aqueous slurry reactors. In addition, a model was developed to elucidate the effects of particle size on the apparent photoactivity of TiO_2 photocatalysts. The model was fit to experimental data obtained in this study, and values for the model parameters were obtained and discussed. Due to the large number of parameters to be evaluated, the model predictions provide a qualitative explanation of the overall trends in the data.

EXPERIMENTAL METHODS

Processing of TiO_2 in Flame Aerosol Reactors

Flame aerosol reactors have been used for processing TiO_2 powders, and the system has been described extensively in previously published papers from our research group (9, 10). A schematic diagram of the system used to process the TiO_2 powders is shown in Fig. 1. The system consists of a diffusion burner, a bubbler vapor generator

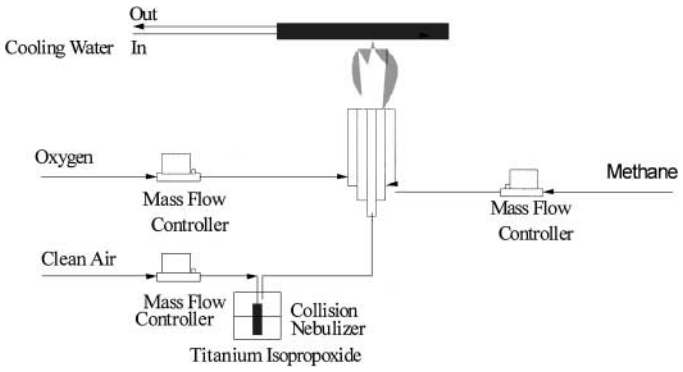

FIG. 1. Schematic diagram of a flame aerosol process for synthesizing TiO_2 powders.

for the TiO_2 precursor, and mass flow controllers to control the flow rates of the gases, including methane, oxygen, and air. TiO_2 was formed on oxidation of the precursor, titanium tetra-isopropoxide (TTIP) (99%, Aldrich Chemical), in the flame and collected thermophoretically on a water-cooled steel plate at a selected distance above the bottom of the flame. The characteristics of the flame-synthesized TiO_2 were controlled by controlling the flow rates of the gases to the flame, the concentration of TTIP introduced into the flame, and the distance at which the TiO_2 was collected. Flame conditions were selected such that the particle sizes of the TiO_2 samples produced in our flame reactor could be controlled. As the flame conditions were well controlled, uniform size particles could be obtained at a fixed distance from the burner nozzle exit (10). Though flame temperatures are very high (>1400°C), the *meta*-stable anatase phase was obtained by quenching the particles on the water-cooled steel collection plate and controlling the time–temperature heating. Details of the crystallinity (9) and the morphological evolution (10) of the TiO_2 powders have been reported elsewhere.

Aliquots of Ishihara ST-01 TiO_2, which is manufactured using a proprietary method, were calcined in air at temperatures ranging from 170 to 700°C for approximately 24 h. The calcined catalysts were also characterized, and their relative photoactivity was determined to investigate the effects of calcination on surface area, crystal size, crystal phase, and photoactivity. Finally, Degussa P25 and Aldrich anatase TiO_2 powders were used as received.

The photocatalysts were characterized with respect to crystal phase and crystal size via X-ray diffraction (XRD), BET surface area, and photoactivity in aqueous systems. The predominant crystal phase of all samples of TiO_2 used in this study was anatase. The fraction of rutile in the flame-synthesized samples was less than 30%. Rutile was not observed in the commercially available TiO_2 (Ishihara ST-01) as received or after calcination at temperatures up to 650°C; approximately 30% rutile was observed in the sample calcined at 700°C. Samples with high rutile content were

not used in establishing the photoactivity for the particle size effects.

Catalyst Characterization

BET surface area. The TiO_2 powders were characterized with respect to BET surface area by nitrogen adsorption at 77 K using a Gemini apparatus (Gemini 2360, Micromeritics, Norcross, GA). Prior to analyses, the TiO_2 samples were degassed at 150°C with a helium purge for approximately 30 min. The adsorption isotherms of nitrogen at 77 K were obtained using eight values of relative pressure ranging from 0.05 to 0.35 and were subsequently used to calculate the BET surface area of each catalyst. The average effective particle size of each TiO_2 catalyst was calculated based upon the BET surface area by assuming nonporous spheres with uniform particle size; a particle size distribution was not measured for these catalysts. However, as stated earlier, flame reactor conditions could be controlled to obtain uniform particle sizes (10).

X-ray diffraction. The crystal phase of each catalyst was determined using a Siemens X-Ray Diffractometer (XRD) with a Cu $K\alpha$ source from $5 < 2\theta < 60$ at a scan rate of 0.1 s^{-1}. The *d*-values of the XRD spectra were used to identify the crystal phases. The Scherrer equation (11) was used to determine the average crystal size of the TiO_2 catalysts. The XRD spectra were used to measure the degree of crystallinity in our samples, and the results are listed in Tables 1 and 2. For the particle size effects on photoactivity, samples with primarily the anatase phase were used.

Uv–vis absorbtion spectroscopy. uv–vis analyses (Shimadzu UV-2501PC) were conducted to determine the light absorption characteristics of each TiO_2 sample. Barium sulfate was used as the reference material. Small amounts of each TiO_2 sample were pressed into pellets of barium sulfate, and the light absorption was measured as a function of wavelength.

Determination of Photoactivity

The photoactivity of each TiO_2 powder was measured in a slurry-type reactor system and has been described in detail elsewhere (12). The reactor in this test system was a 25-cm^3 impinger (Pyrex, Ace Glass) placed vertically in a water bath (500-cm^3 Pyrex beaker). The Pyrex filtered out wavelengths of less than 300 nm, and the water bath filtered out infrared wavelengths from the lamp. Aeration flow to the reactor was pure oxygen controlled at 150 cm^3 min^{-1}. Samples (1/2 cm^3 each) were taken at 15- to 20-min intervals. The phenol in each aqueous sample was extracted with benzene (99%, Aldrich Chemical) and analyzed using a Hewlett–Packard HP 5890 gas chromatograph (GC) equipped with an FID detector and capillary column (DB-5, J&W Scientific). The lamp used for photocatalysis was a 450-W xenon lamp (Oriel Instruments), positioned horizontally with respect to and in very close proximity to the impinger.

For each experiment, up to 2.5 g/L TiO_2 was used to prepare slurries with phenol solution (approximately 1.4 mM). The phenol was obtained from Fischer Scientific (99% pure). The slurries were sonicated for up to 5 min prior to each test. Samples were taken from the reaction mixture at 15-min intervals for up to 1 h. Control experiments indicated that no significant reactions with phenol occur on TiO_2 in the dark, and that no significant homogeneous photolysis reactions with phenol occur in the absence of TiO_2 in our test system.

TABLE 1

Summary of Flame-Synthesized TiO_2 Used in This Study

Combustion gas flow rates (LPM)			Collection distance (cm)	TTIP temp. (C)	Fraction anatase TiO_2	BET surface area (m^2/g)	BET particle size (nm)
Methane	Oxygen	Air					
0.4	0.2	2.5	5	23	1.0	265	6
1.5	4.5	2.5	15	53	0.81	120	12
1.2	2.0	3.0	8	23[a]	0.91	50	30
1.2	2.5	3.0	4	23[a]	0.73	30	48

[a] TTIP was introduced as both vapor and aerosol.

TABLE 2

Summary of Ishihara ST-01, Degussa P25, and Aldrich Anatase TiO_2

TiO_2	Calcination temp. (C)	Duration of calcination (h)	Fraction anatase TiO_2	BET surface area (m^2/g)	BET particle size (nm)
Ishihara ST-01	As received	—	1	300	5
	400	24	1	100	16
	500	24	1	67	22
	550	24	1	53	28
	600	24	1	35	42
	650	24	1	25	60
Degussa P25	As received	—	0.8	50	30
Aldrich anatase	As received	—	1	10	169

MODEL DEVELOPMENT

To predict the overall trends of photoactivity as a function of particle size, a phenomenonlogical model was developed. The photocatalytic oxidation reactions that are often described for irradiated slurries of TiO_2 are (6, 12–14)

$$TiO_2 + h\nu \rightarrow e^- + h^+, \quad [1]$$

$$e^- + h^+ \rightarrow \text{heat}, \quad [2]$$

$$e^- + O_{2,ads} \rightarrow O_2^-, \quad [3]$$

$$h^+ + H_2O_{ads} \rightarrow \bullet OH + H^+, \qquad [4]$$
$$h^+ + OH^-_{ads} \rightarrow \bullet OH,$$

$$\bullet OH + RH_{ads} \rightarrow \bullet R + H_2O, \qquad [5]$$

$$\bullet OH + X_{i,ads} \rightarrow X_i \bullet + H_2O, \qquad [6]$$
$$\bullet OH + X_{i,ads} \rightarrow X_j,$$

$$\bullet OH + Y_{i,ads} \rightarrow Y_j, \qquad [7]$$

where the subscript ads refers to adsorbed species on the titania particles.

Equation [1] represents the rate of electron–hole formation in the TiO_2 particles on irradiation with light. This rate is dependent on the light absorption profile and the primary quantum yield, both of which are dependent on the incident light profile and on the optical and physical properties of the TiO_2 particles. The reactor geometry and size and TiO_2 concentration affect the incident light profile throughout the reactor, and so they are significant factors in the observed rates of reaction. Equation [2] represents the rate of electron–hole recombination that occurs on the surfaces of the particles (6). RH, X_i, and Y_i represent the organic substrate, the organic radical species and organic partial oxidation products, and the inorganic radicals and species, respectively, in the reaction slurry that compete with the organic substrate for reaction with hydroxyl radicals. Details of the model development are discussed in the literature (6, 12, 13).

The equations above were used to derive relationships between the concentrations of photogenerated species on the TiO_2 particles and the effective primary particle sizes of the TiO_2 powders. For this analysis, it was assumed that all particles were spherical, nonporous, and uniform in size.

The rate of photooxidation of an organic substrate in an aqueous slurry can be represented by

$$\frac{dC_{RH}}{dt} = -k_5[\bullet OH]K_{RH}C_{RH}(a_sN), \qquad [8]$$

where C_{RH} is the concentration of organic substrate in the reaction slurry, [•OH] is the concentration of hydroxyl radicals on the surface of the titania particles, K_{RH} is the adsorption coefficient of the organic substrate on TiO_2, k_5 is the intrinsic reaction rate constant for the hydroxyl radical and the organic substrate, a_s is the surface area of the TiO_2 particles, and N is the number of TiO_2 particles per unit volume. Note that this model was developed under the assumption that adsorption equilibrium occurs instantaneously, and Eq. [8] is valid under such conditions. N can be determined according to the expression

$$N = \frac{C_{TiO_2}}{\rho_{TiO_2}v_p}, \qquad [9]$$

where ρ_{TiO_2} is the density of anatase titanium dioxide, v_p is the volume of a particle, and C_{TiO_2} is the concentration of TiO_2 in the reaction slurry.

The light intensity profile within the reactor can significantly affect the apparent photoactivity of the TiO_2, and in batch slurry reactors, scattering effects cannot be ignored (15). The kinetic data acquired in this study are volume-averaged concentrations of phenol in the reaction slurry as a function of time. However, the photooxidation of phenol occurs only at particle surfaces that are irradiated with light ($\lambda \leq 380$ nm), which varies with light penetration depth into the reaction slurry. Since the reaction slurry was well mixed during the reaction, the samples that were taken from the reaction slurry represent volume-averaged samples. Several studies have been published regarding the light absorption and light intensity profiles in TiO_2 slurries, and detailed models have been developed in this regard (14). In this model, however, the electron–hole generation in the reaction slurry as a function of light penetration depth was approximated using extinction theory (16).

The rate of electron–hole generation was represented by the expression

$$G(z) = k_1 I(z) \alpha A_p, \qquad [10]$$

where $G(z)$ is the rate of electron–hole generation as a function of depth z in the reaction slurry, $I(z)$ is the light intensity at depth z, α is the light absorption efficiency for TiO_2, and A_p is the projected area of the particle. Using the extinction theory (16), the light intensity for monochromatic light can be expressed as

$$I(z) = I_o \exp(-bz), \qquad [11]$$

where b is the light extinction coefficient and I_o is the light intensity incident on the reactor. The extinction coefficient can be expressed as

$$b = NA_pQ_{ext} = NA_p(Q_{abs} + Q_{scattering}), \qquad [12]$$

where Q_{ext}, Q_{abs}, and $Q_{scattering}$ are efficiencies of extinction, absorption, and scattering, respectively. Light scattered from other particles will also be incident on the remaining suspension; however, this intensity is very small compared to the incident light intensity (which undergoes extinction due to scattering and absorption). Expressions for Q_{abs} and $Q_{scattering}$ are (16, 17)

$$Q_{abs} = \frac{-4\pi d_p}{\lambda}\mathrm{Im}\left\{\frac{m^2-1}{m^2+2}\right\} = k_a d_p,$$
$$Q_{scattering} = \frac{8\pi^4 d_p^4}{3\lambda^4}\mathrm{Re}\left\{\frac{m^2-1}{m^2+2}\right\}^2 = k_s d_p^4, \qquad [13]$$

where λ is the wavelength of absorbable and scattered light, m is the refractive index of TiO_2 in water, Im means that the imaginary part of the refractive index must be considered, and Re means that only the real part of the refractive index

is used. k_a and k_s are absorption and scattering coefficients, respectively, that depend on the refractive index and wavelength of absorbable light. k_a and k_s are used in subsequent equations for simplicity. Assuming that α is expressed similarly to Q_{abs}, and using Eq. [9] and Eqs. [11]–[13], Eq. [10] can be expanded:

$$G(z) = \frac{k_1 k_a' I_o \pi d_p^3}{4} \exp\left(-\frac{3C_{\text{TiO}_2}}{2\rho_{\text{TiO}_2}}\left[k_a + k_s d_p^3\right] z\right). \quad [14]$$

To obtain the overall rate of electron–hole generation in the reaction slurry, Eq. [14] was integrated between the limits of 0 and L, where L is dependent on the physical dimensions of the reactor system:

$$G_{\text{total}} = \frac{k_1 k_a I_o \pi \rho_{\text{TiO}_2} d_p^3}{6C_{\text{TiO}_2}\left[k_a + k_s d_p^3\right]} \times \left[1 - \exp\left(\left(\frac{-3C_{\text{TiO}_2}}{2\rho_{\text{TiO}_2}}\right)\left[k_a + k_s d_p^3\right] L\right)\right]. \quad [15]$$

Adsorption of the organic substrate, dissolved oxygen, and water occur on all particles within the reaction slurry, and since particles are well mixed in the reaction slurry, the model was developed further by using an average rate of electron–hole generation per particle. The average rate of electron–hole generation per particle in the reaction slurry was approximated by dividing G_{total} (Eq. [15]) by N (Eq. [9]). After simplification, the average rate of electron–hole generation per particle in the reaction slurry can be expressed as

$$g_{\text{avg}} = \frac{k_g d_p^6}{\left(C_{\text{TiO}_2}\right)^2\left[1 + Rd_p^3\right]}\left[1 - \exp\left(-\sigma C_{\text{TiO}_2}\left(1 + Rd_p^3\right)\right)\right], \quad [16]$$

where g_{avg} is the average rate of electron–hole generated per particle in the reaction slurry, and k_g, R, and σ are parameters that are defined as follows:

$$k_g = \frac{k_1 k_a' I_o \pi^2 \rho_{\text{TiO}_2}^2}{36 k_a}, \quad [17]$$

$$R = \frac{k_s}{k_a}, \quad [18]$$

$$\sigma = \frac{3k_a L}{2\rho_{\text{TiO}_2}}. \quad [19]$$

The model was further developed on a per-particle basis using a kinetic analysis very similar to those developed previously (12–14). Assuming photostationary state for aqueous-phase irradiated TiO_2 slurries, the following expressions were obtained on a per particle basis:

$$\begin{aligned}\frac{d[e^-]}{dt} &= \frac{k_g d_p^6\left(1 - \exp\left(-\sigma C_{\text{TiO}_2}\left(1 + Rd_p^3\right)\right)\right)}{\left(C_{\text{TiO}_2}\right)^2\left(1 + Rd_p^3\right)} \\ &\quad - k_2[e^-][h^+](a_s) - k_3[e^-]C_{\text{O}_2,\text{ads}}(a_s) \approx 0, \\ [e^-] &= \frac{k_g d_p^6\left(1 - \exp\left(-\sigma C_{\text{TiO}_2}\left(1 + Rd_p^3\right)\right)\right)}{\left(C_{\text{TiO}_2}\right)^2\left(1 + Rd_p^3\right)\left(k_2[h^+]\pi d_p^2 + k_3 K_{\text{O}_2} C_{\text{O}_2}\pi d_p^2\right)} \\ &= \frac{k_g d_p^4\left(1 - \exp\left(-\sigma C_{\text{TiO}_2}\left(1 + Rd_p^3\right)\right)\right)}{\left(C_{\text{TiO}_2}\right)^2\left(1 + Rd_p^3\right)\pi\left(k_2[h^+] + k_3 K_{\text{O}_2} C_{\text{O}_2}\right)};\end{aligned} \quad [20]$$

$$\begin{aligned}\frac{d[h^+]}{dt} &= \frac{k_g d_p^6\left(1 - \exp\left(-\sigma C_{\text{TiO}_2}\left(1 + Rd_p^3\right)\right)\right)}{\left(C_{\text{TiO}_2}\right)^2\left(1 + Rd_p^3\right)} \\ &\quad - k_2[e^-][h^+](a_s) - k_4 C_{\text{H}_2\text{O},\text{ads}}[h^+](a_s) \approx 0, \\ [h^+] &= \frac{k_g d_p^6\left(1 - \exp\left(-\sigma C_{\text{TiO}_2}\left(1 + Rd_p^3\right)\right)\right)}{\left(C_{\text{TiO}_2}\right)^2\left(1 + Rd_p^3\right)\left(k_2[e^-]\pi d_p^2 + k_4 K_{\text{H}_2\text{O}} C_{\text{H}_2\text{O}}\pi d_p^2\right)} \\ &= \frac{k_g d_p^4\left(1 - \exp\left(-\sigma C_{\text{TiO}_2}\left(1 + Rd_p^3\right)\right)\right)}{\left(C_{\text{TiO}_2}\right)^2\left(1 + Rd_p^3\right)\pi\left(k_2[e^-] + k_4 K_{\text{H}_2\text{O}} C_{\text{H}_2\text{O}}\right)};\end{aligned} \quad [21]$$

$$\begin{aligned}\frac{d[\bullet\text{OH}]}{dt} &= k_4[h^+]C_{\text{H}_2\text{O},\text{ads}}(a_s) - k_5[\bullet\text{OH}]C_{RH,\text{ads}}(a_s) \\ &\quad - \sum k_{6i}[\bullet\text{OH}]C_{x_i,\text{ads}}(a_s) \\ &\quad - \sum k_{7j}[\bullet\text{OH}]C_{Y,\text{ads}}(a_s) \approx 0, \\ [\bullet\text{OH}] &= \frac{k_4 K_{\text{H}_2\text{O}}[h^+]C_{\text{H}_2\text{O}}}{k_5 K_{RH} C_{RH} + \sum k_{6i} K_{X_i} C_{X_i} + \sum k_{7_j} K_{Y_i} C_{Y_i}}.\end{aligned} \quad [22]$$

In the expressions above, d_p is the effective diameter of the TiO_2 particles (based upon BET surface area), a_s is the surface area of the particles, C_{RH} (mM) is the concentration of the organic substrate, I_o (einsteins/s) is the incident light intensity, $C_{\text{H}_2\text{O}}$ (mM) is the concentration of water, C_{O_2} (mM) represents the dissolved oxygen, $[e^-]$ and $[h^+]$ (ions/surface area of catalyst) are the concentrations of electrons and holes in TiO_2 particles, and [OH] (radicals/surface area of catalyst) is the hydroxyl radicals concentration on the surface of the irradiated TiO_2 particles. K_{RH}, $K_{\text{H}_2\text{O}}$, K_{Xi}, K_{Yj}, and K_{O_2} are the equilibrium adsorption coefficients, and k_i are the reaction rate constants for their respective reactions shown above.

Using Eqs. [20] and [21] to derive an expression for the concentration of photogenerated holes on the TiO_2 particles, a quadratic expression is obtained:

$$[h^+]^2 + \left\{\frac{k_3 K_{\text{O}_2} C_{\text{O}_2}}{k_2}\right\}[h^+] - \frac{k_g k_3 K_{\text{O}_2} C_{\text{O}_2} d_p^4\left(1 - \exp\left(-\sigma C_{\text{TiO}_2}\left(1 + Rd_p^3\right)\right)\right)}{k_2 k_4 K_{\text{H}_2\text{O}} C_{\text{H}_2\text{O}}\pi\left(C_{\text{TiO}_2}\right)^2\left(1 + Rd_p^3\right)} \approx 0. \quad [23]$$

Solving Eq. [23] for $[h^+]$, Eq. [24] is obtained:

$$[h^+] = \left\{ -1 + \sqrt{1 + \frac{4k_g k_2 d_p^4 \left(1 - \exp\left(-\sigma C_{TiO_2}\left(1 + Rd_p^3\right)\right)\right)}{\left(C_{TiO_2}\right)^2 \left(1 + Rd_p^3\right) \pi k_3 K_{O_2} C_{O_2} k_4 K_{H_2O} C_{H_2O}}} \right\} \times \frac{k_3 K_{O_2} C_{O_2}}{2k_2}. \quad [24]$$

Substituting Eq. [24] into Eq. [22], and subsequently into Eq. [8], the resulting equation for the photooxidation of organic substrates is expressed as follows:

$$-\frac{dC_{RH}}{dt} = \frac{\frac{3k_5 K_{RH} C_{RH} k_3 K_{O_2} C_{O_2} k_4 K_{H_2O} C_{H_2O} C_{TiO_2}}{k_2 \rho_{TiO_2} d_p} \left\{ -1 + \sqrt{1 + \frac{4k_g k_2 d_p^4 (1 - \exp(-\sigma C_{TiO_2}(1 + Rd_p^3)))}{\left(C_{TiO_2}\right)^2 (1 + Rd_p^3) \pi k_3 K_{O_2} C_{O_2} k_4 K_{H_2O} C_{H_2O}}} \right\}}{k_5 K_{RH} C_{RH} + \sum k_{6i} K_{X_i} C_{X_i} + \sum k_{7_j} K_{Y_i} C_{Y_i}}. \quad [25]$$

Assuming an initial rate of reaction, at which $k_5 K_{RH} C_{RH} + \sum k'_{6i} K_{Xi} C_{Xi}$ can be approximated as $k_5 K_{RH} C_{RHo}$, where C_{RHo} is the initial substrate concentration, and assuming that Y_i species are photogenerated and at photostationary state, and adsorbed oxygen and water concentrations are constant, the expression above can be simplified to

$$-\frac{dC_{RH}}{dt} = \frac{aC_{RH} C_{TiO_2}}{d_p (C_{RHo} + b)} \times \left[-1 + \sqrt{1 + \frac{cd_p^4 \left(1 - \exp\left(-\sigma C_{TiO_2}\left(1 + Rd_p^3\right)\right)\right)}{\left(C_{TiO_2}\right)^2 \left(1 + Rd_p^3\right)}} \right], \quad [26]$$

where

$$a = \frac{3k_3 K_{O_2} C_{O_2} k_4 K_{H_2O} C_{H_2O}}{k_2 \rho_{TiO_2}}, \quad [27]$$

$$b = \frac{\Sigma k_{7_j} Y_j}{k_5 K_{RH}}, \quad [28]$$

$$c = \frac{4k_g k_2}{k_3 K_{O_2} C_{O_2} k_4 K_{H_2O} C_{H_2O} \pi}. \quad [29]$$

Equation [26] was used to fit the data from the photoactivity experiments, and values for parameters a, b, c, R, and σ were obtained. Due to the large number of parameters that were determined by comparison to experiments, the model provides an overall description of the variation of photoactivity as a function of particle size.

RESULTS AND DISCUSSION

Catalyst Synthesis

The synthesis method is a critical factor in the ultimate photoactivity of TiO_2 (1, 2). In this study, TiO_2 was synthesized using a flame aerosol process. The advantages of the flame aerosol process are that the crystal phase and particle size can be varied by controlling the conditions of the flame and collection surface, and that the resulting TiO_2 powders do not require a calcination step to achieve crystallinity.

A summary of the TiO_2 samples that were used in this study is provided in Tables 1 and 2. Noted in Table 1 is the wide variation in effective particle sizes of anatase TiO_2 attainable using the flame aerosol process without subsequent calcination. Controlling the gas flow rates results in differing residence times, and so does the location of the collection plate. Due to the different residence times in the flame zone, the growth rates are altered, thus resulting in the different sizes that were obtained. The temperature history is also altered, and hence the crystal phase of the resultant powders could be controlled. A detailed description of this is provided in the paper by Yang *et al.* (9).

Catalyst Characterization

The particle size of each TiO_2 powder was calculated using the BET surface area assuming nonporous spherical particles of uniform particle size; the results are tabulated in Tables 1 and 2. The anatase crystal size of each TiO_2 powder was calculated using XRD spectra, with selected spectra shown in Fig. 2, and the Scherrer equation. Notable in the XRD spectra is the fact that the anatase peaks sharpen and increase in intensity as the crystal size increases in both flame-synthesized TiO_2 and calcined Ishihara ST-01 TiO_2. The agreement between the BET particle size and XRD crystal size for flame-synthesized and Ishihara TiO_2 samples are shown in Fig. 3, top and bottom, respectively.

The agreement between the particle sizes calculated using the BET surface area and the XRD spectra is very good for the flame-synthesized TiO_2, where the slope between them is 1.06 (Fig. 3, top). The reason for this excellent agreement is because in the flame process, the particles are formed and sinter rapidly in the flame, completely merging the particles involved, as indicated in a previous study (9). However, sintering slows down significantly as temperature decreases above the flame, and primary particles can be distinguished on TEM micrographs of the TiO_2 powders, as shown in Fig. 4. Although agglomeration does occur as the particles cool above the flame, the agglomeration does not significantly affect the BET surface area of the TiO_2 powders (5).

The calcined Ishihara ST-01 shows poor correlation between the BET particle size and the XRD crystal size, especially at the higher effective particle sizes. As shown

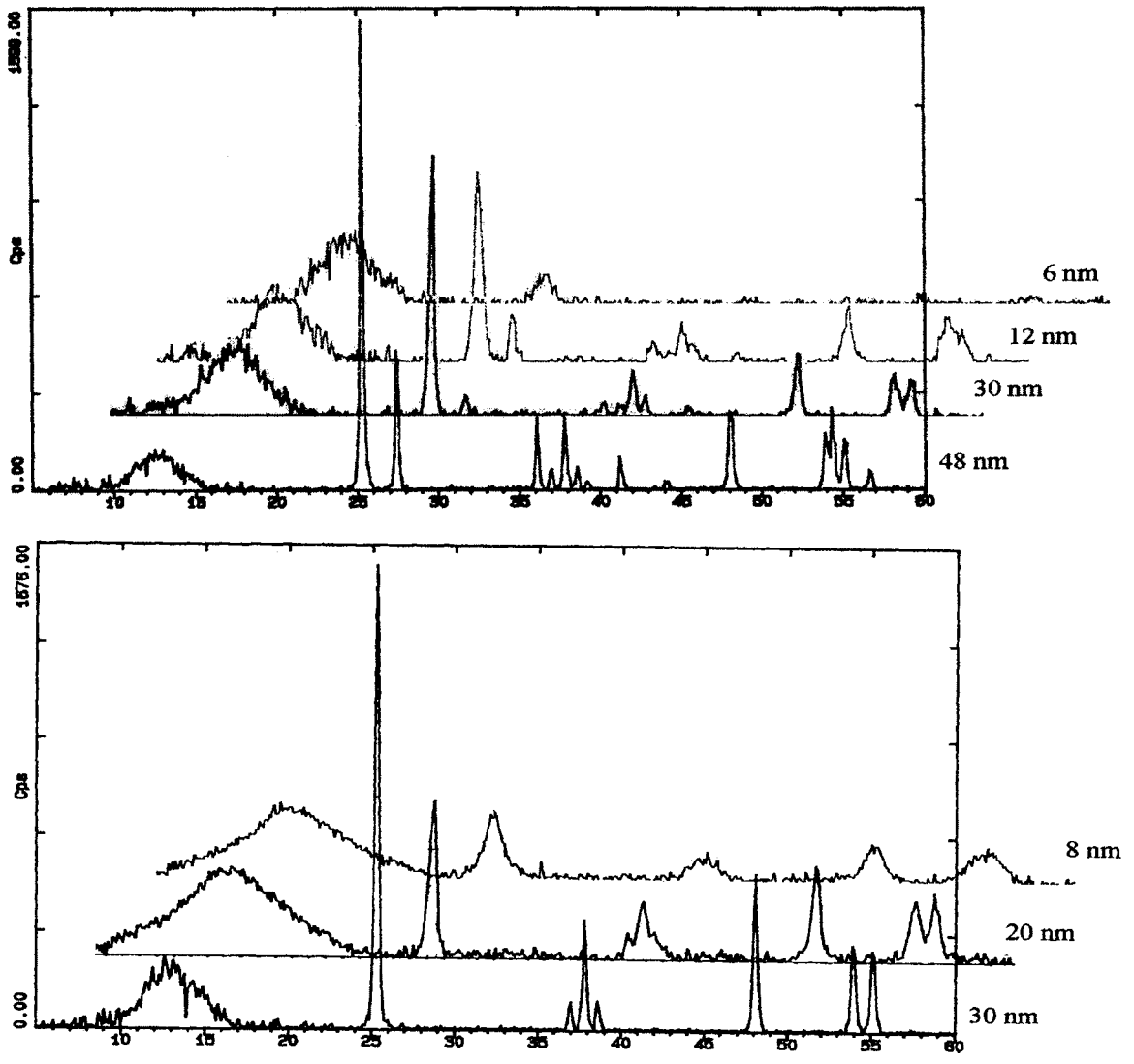

FIG. 2. XRD spectra as a function of particle size. (top) Flame-synthesized TiO_2, and (bottom) Ishihara ST-01 TiO_2 as received and calcined.

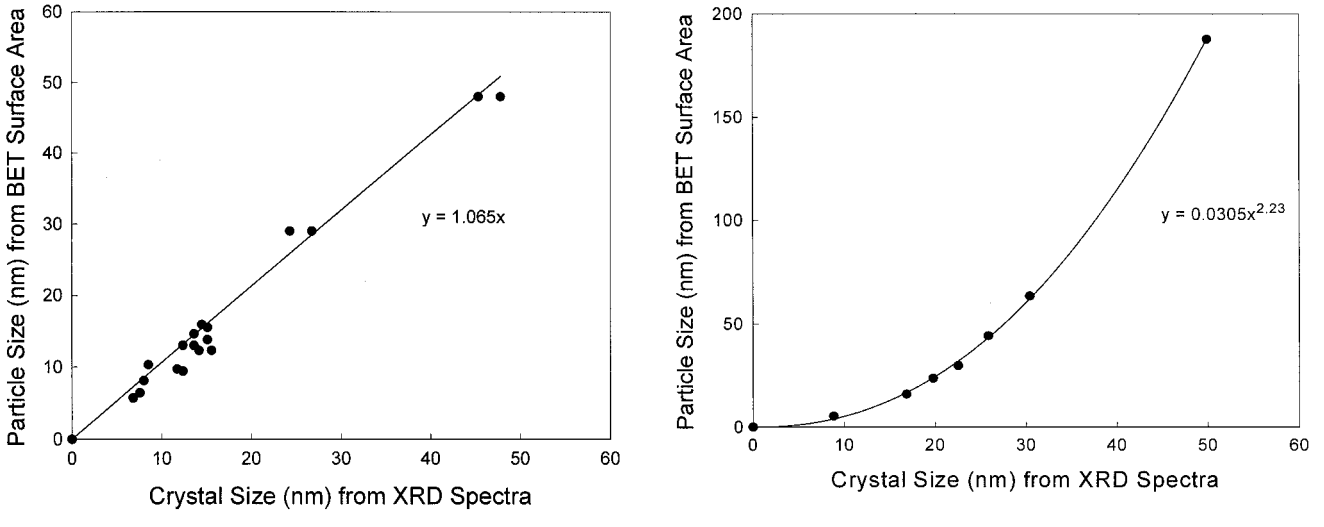

FIG. 3. Agreement between effective particle size (from BET surface area) and crystal size (from XRD spectra). (left) Flame synthesized and (right) annealed Ishihara.

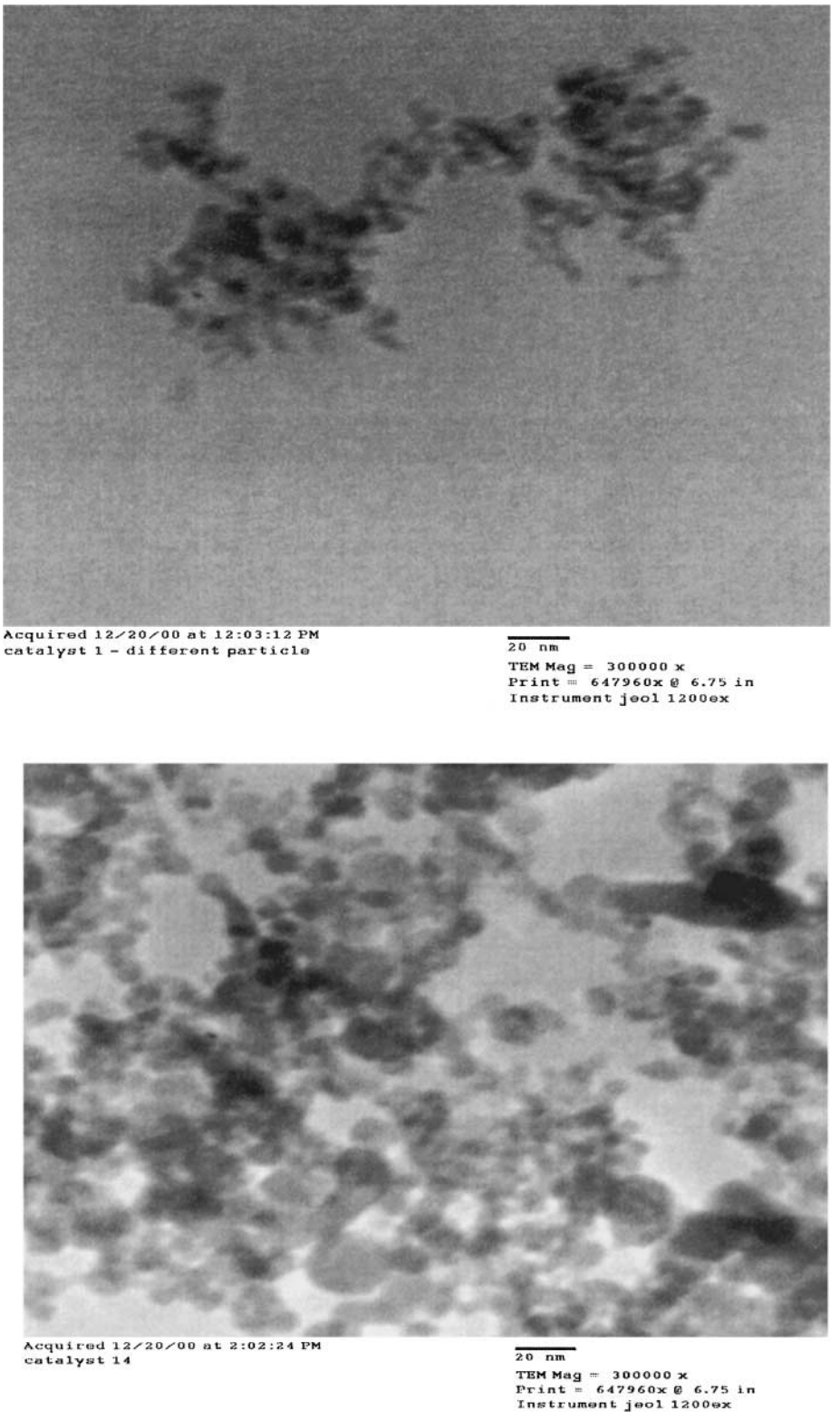

FIG. 4. TEM micrographs of flame-synthesized TiO_2: (top) 6 and (bottom) 15 nm.

in Fig. 3, right, the effective particle size calculated from the BET surface area appears to be a power function of the XRD crystal size. This can be explained by the fact that the TiO_2 particles underwent densification during calcination, which increases the effective particle size based on BET surface area. The rate of densification is generally modeled as a power function of the initial particle size. Densification reduced the surface area of the Ishihara TiO_2 at a faster rate than crystal growth occurred within the TiO_2 particles. This is apparent by comparing the SEM analyses of Ishihara ST-01 as received (Fig. 5, top) and after calcination at 500 C (Fig. 5, bottom). In Fig. 5, bottom, the TiO_2 primary particles appear to have merged together, thus lowering the surface area of the powder.

Photoactivity: Oxidation of Phenol

The apparent photoactivity of TiO_2 for the photooxidation of phenol as a function of average effective particle size is shown in Figs. 6a and 6b for the different samples. The apparent photoactivity increased as the effective particle size increased from 5 to approximately 30 nm and decreased as the effective particle size increased beyond 30 nm. The fact that the optimum particle size with respect

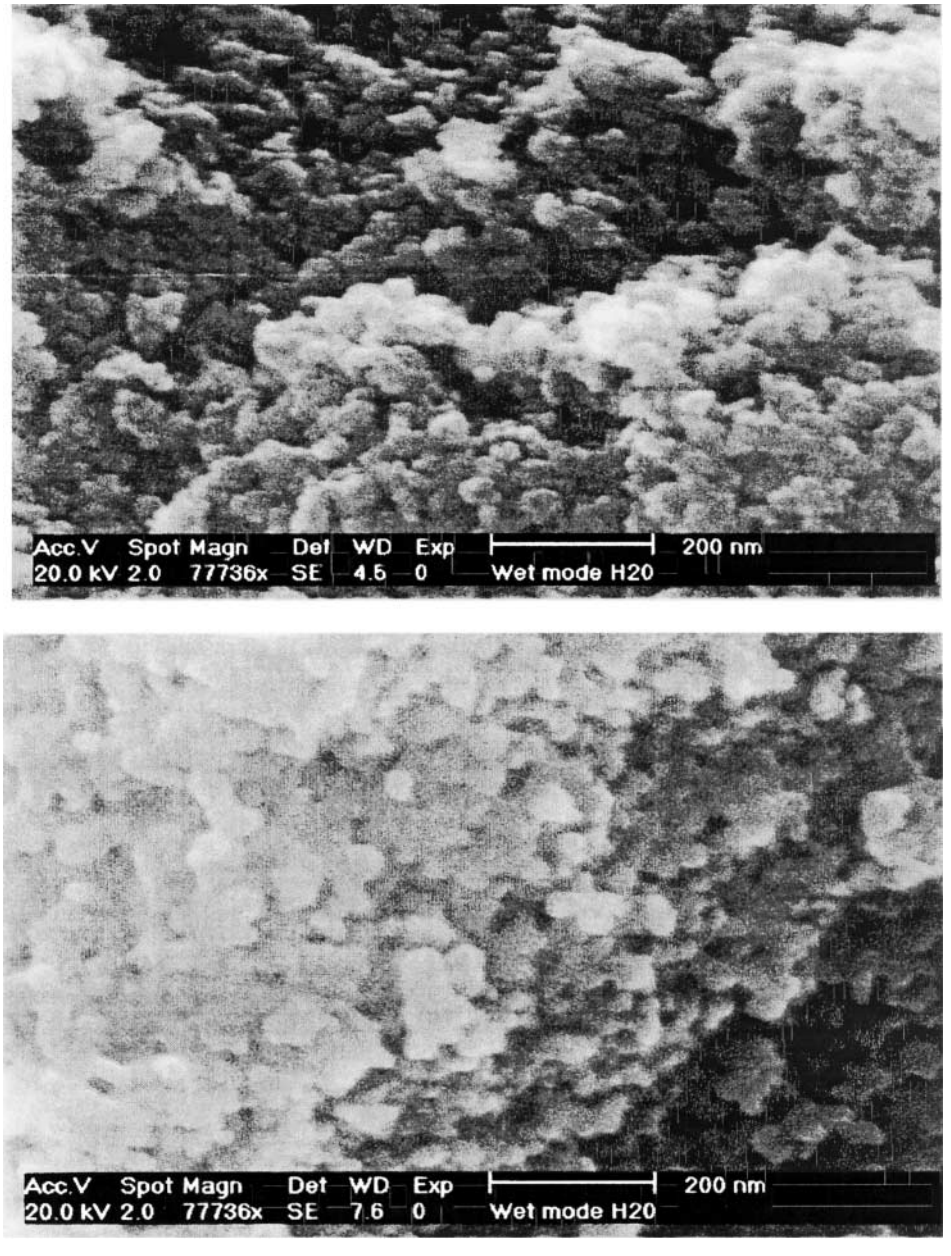

FIG. 5. SEM micrographs of Ishihara ST-01 (top) as received and (bottom) after being calcined at 500°C in air for 24 h.

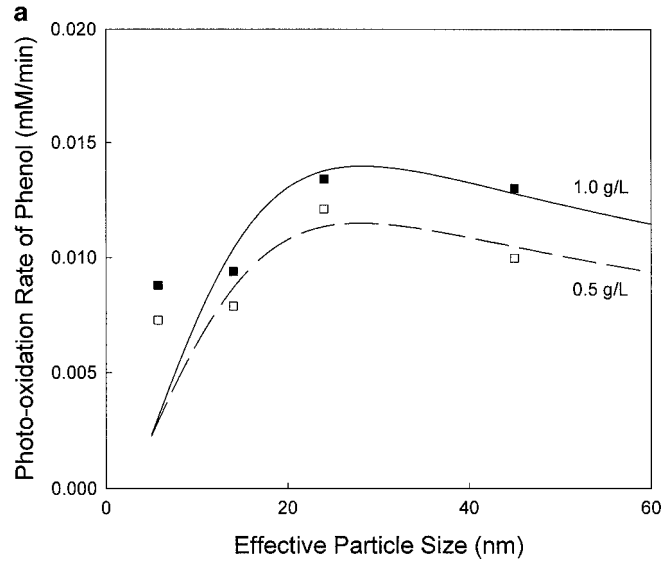

FIG. 6a. Apparent photooxidation rate of phenol in a batch slurry reactor for flame-synthesized TiO_2.

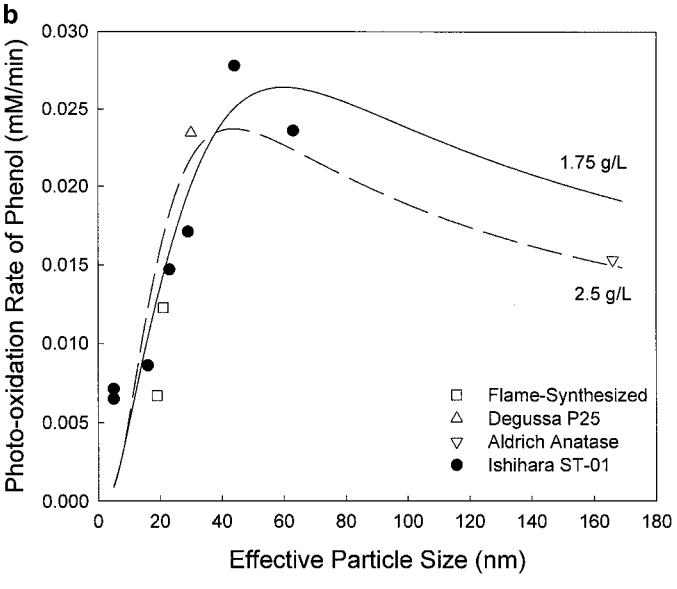

FIG. 6b. Apparent photooxidation rate of phenol in a batch slurry for commercially available and selected flame-synthesized TiO_2.

to apparent photoactivity was 25 to 40 nm in all sets of photocatalysis experiments conducted in this study is noteworthy. Using Fig. 3 to correlate the effective particle size to XRD crystal size, it is also noteworthy that the optimum anatase crystal size with respect to photoactivity is 25 nm in all cases. This suggests that the optical (light absorption and scattering) and electrical properties of TiO_2 at effective particle sizes less than ~40 nm and anatase crystal sizes less than 25 nm dominate the apparent photoactivity of TiO_2, but at effective particle sizes greater than ~30 nm and anatase crystal sizes greater than 25 nm, the optical and electrical properties of TiO_2 become similar to those of bulk TiO_2, and the apparent photoactivity of TiO_2 has dominated by its available surface area.

The band gap energy, ΔE, was determined from the *uv–vis* absorbtion spectra of the different samples of TiO_2 (Figs. 7a and 7b) and plotted as a function of particle size in Fig. 8. The solid line in Fig. 8 was calculated using expressions from the literature for ΔE vs particle size (18–20). Significant size quantization effects are predicted for anatase TiO_2 below sizes of 14 nm (21) and this is consistent with our measured values. While the estimated size of 14 nm does not exactly match the size at which maximum photoactivity is observed (~30 nm), it does provide qualitative support to the reactivity data. Raman spectra of the samples as a function of particle size (21, 22) also provide support for these observations.

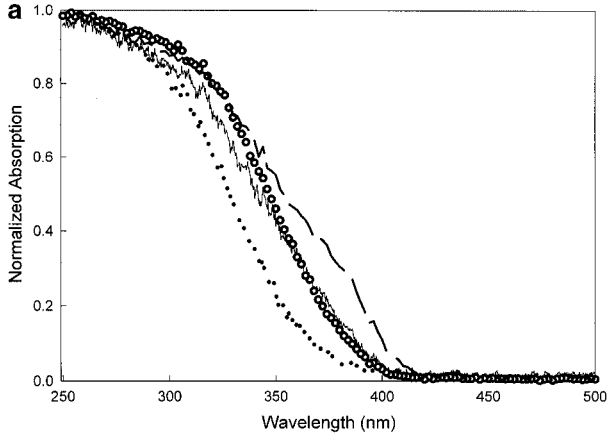

FIG. 7a. *Uv–vis* absorption spectra of flame-synthesized TiO_2 powders of different particle sizes. ●, 6 nm; ——, 12 nm; ○, 30 nm; - - - -, 48 nm.

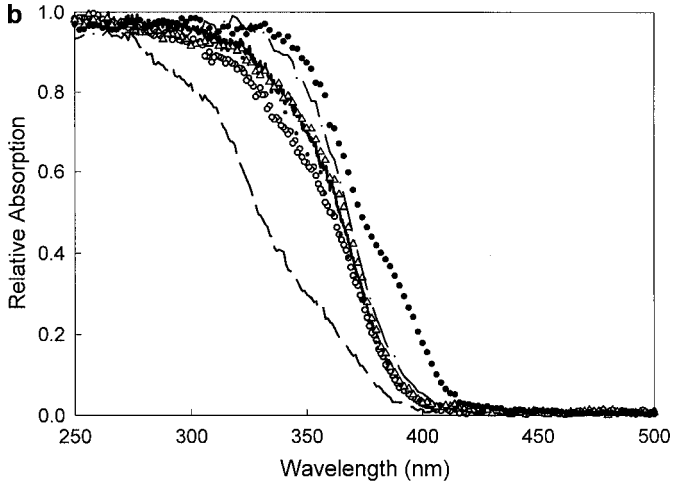

FIG. 7b. *Uv–vis* absorbtion spectra of Ishihara ST-01 TiO_2 powders as received and calcined to obtain different particle sizes. - - -, 5 nm; ○, 16 nm; •, 22 nm; △, 28 nm; –, 42 nm; —·—, 60 nm; ●, 89 nm.

TABLE 3

Summary of Parameter Values Used to Model Experimental Data Shown in Figs. 6a and 6b

TiO_2 sample	Different samples of TiO_2[a]	Ishihara ST-01 as received and calcined TiO_2	Flame-synthesized TiO_2	
TiO_2 concentration (g/L)	2.5	1.75	1.0	0.5
Phenol concentration (mM)	1.4	1.4	1.34	1.34
Parameter a	9.75×10^{-10}	9.75×10^{-10}	9.75×10^{-10}	9.75×10^{-10}
Parameter b	40	60	75	65
Parameter c	1.1×10^{33}	1.3×10^{33}	2.95×10^{34}	1.47×10^{34}
Parameter σ	5×10^{7}	5×10^{7}	5×10^{7}	5×10^{7}
Parameter R	3×10^{22}	1×10^{22}	1×10^{23}	1×10^{23}

[a] Degussa P25, Aldrich anatase, and Ishihara ST-01 as received and two flame-synthesized samples of TiO_2.

The model parameters that were used to generate the curves in Figs. 6a and 6b are shown in Table 3. Noted is the fact that the same values for parameters a and σ were used for all four curves. This was done because the constants that comprise parameter a are reaction rate constants for photogenerated and adsorbed species, which should be independent of the source, concentration, and particle size of TiO_2, and parameter σ is a function of the refractive index of TiO_2, which should not change if the crystal phase is anatase. Differences in the extent of adsorption of water, oxygen, and the organic substrate (phenol in this study) on the Ishihara, Degussa, Aldrich, and flame-synthesized TiO_2 may account for differences in parameters b and c. Parameter c also contains the terms for electron–hole pair generation, which are strongly dependent on the physical and optical properties and concentration of the TiO_2 and light intensity profile in the reaction slurry. Therefore, a significant difference in the value of parameter c for the commercially available and flame-synthesized TiO_2 powders was noted. Parameter R, the ratio of light scattering and absorption coefficients, also varied. The differences in R may be due to the effects of particle agglomeration, which were not accounted for in this study but would have an effect on light scattering.

Noted, too, is that the model consistently underpredicts the apparent photooxidation rate of phenol at particle sizes less than 10 nm. This appears to be a systemic error in the model and may be a result of nonuniform effective particle sizes, where the presence of larger particles would skew the experimental results to show higher than predicted photooxidation rates of phenol. In addition, photolysis of phenol would skew the experimental results to show higher than predicted photooxidation rates of phenol at very small particle sizes; however, photolysis of phenol was neither expected at light wavelengths greater than 300 nm nor observed in control runs conducted in this study. Due to the large number of parameters that have to be estimated, it should be stated that the model only provides for an overall explanation of trends as a function of particle size.

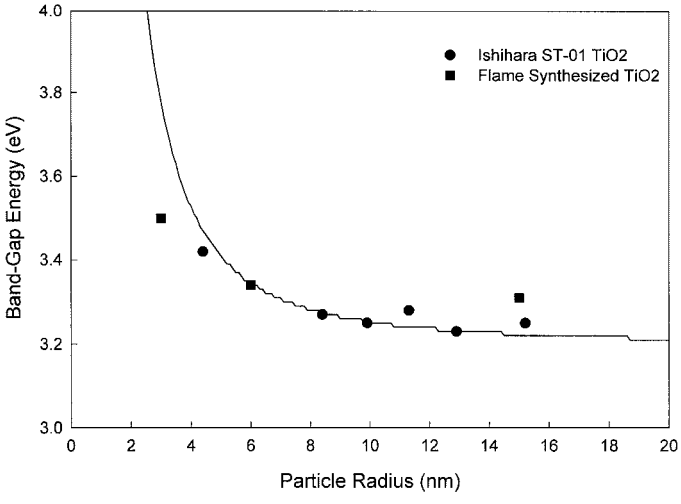

FIG. 8. Band gap energy as a function of particle size. (Solid line) Prediction based on equations in the literature (18–20) showing size quantization effects.

CONCLUSIONS

The effect of particle size on the apparent photoactivity of titanium dioxide (TiO_2) in water for photooxidation reactions is significant, especially at effective particle sizes of less than 30 nm. At effective particle sizes of less than ~30 nm, the apparent photoactivity increases sharply with particle size, likely due to the significant effects of particle size on the efficiency at which light is absorbed and the photogenerated charge-carrier dynamics within the particle in this size range. The results of this study showed an optimum effective particle size ranging from 25 to 40 nm and an optimum anatase crystal size of 25 nm in all cases. The optimum particle and crystal sizes are a result of a strong dependence of light absorption and scattering efficiencies and charge-carrier dynamics on particle size at particle sizes of less than 30 nm. At effective particle sizes greater than 30 nm, the surface area available for redox reactions becomes much

more important in predicting the apparent photoactivity of TiO_2 powders, and so, the apparent photoactivity decreases with increasing particle size above 30 nm.

REFERENCES

1. Schiavello, M., "Heterogeneous Photocatalysis," Vol. 3. Wiley, New York, 1997.
2. Sclafani, A., Palmisano, L., and Schiavello, M., *J. Phys. Chem.* **94**, 829 (1990).
3. Wang, C.-C., Zhang, Z., and Ying, J. Y., *Nanostruct. Mater.* **9**, 583 (1997).
4. Zhang, Z., Wang, C., Zakaria, R., and Ying, J., *J. Phys. Chem. B* **102**, 10871 (1998).
5. Maira, A. J., Yeung, K. L., Lee, C. Y., Yue, P. L., and Chan, C. K., *J. Catal.* **192**, 185 (2000).
6. Gerischer, H., *Electrochim. Acta* **40**(10), 1277 (1995).
7. Grela, M., and Colussi, A. J., *J. Phys. Chem.* **100**, 18214 (1996).
8. Xu, N., Shi, Z., Fan, Y., Dong, J., Shi, J., and Hu, M. Z.-C., *Ind. Eng. Chem. Res.* **38**, 373 (1999).
9. Yang, G. X., Zhuang, H. R., and Biswas, P., *Nanostruct. Mater.* **7**(6), 675 (1996).
10. Yang, G., and Biswas, P., *Aerosol Sci. Technol.* **27**, 507 (1997).
11. Doss, C. J., and Zallen, R., *Phys. Rev. B* **48**(21), 15626 (1993).
12. Almquist, C. L. B., and Biswas, P., *Chem. Eng. Sci.* **56**(11), 3421 (2001).
13. Turchi, C. S., and Ollis, D. F., *J. Catal.* **122**, 178 (1990).
14. Alfano, O. M., Cabrera, M. I., and Cassano, A. E., *J. Catal.* **172**, 370 (1997).
15. Cabrera, M. I., Alfano, O. M., and Cassano, A. E., *J. Phys. Chem.* **100**(51), 20043 (1996).
16. Hinds, W. C., "Aerosol Technology, Properties, Behaviour, and Measurement of Airborne Particles." Wiley, New York, 1982.
17. Friedlander, S. K., "Smoke, Dust, and Haze: Fundamentals of Aerosol Behavior." Oxford Univ. Press, New York, 2000.
18. Serpone, N., Lawless, D., and Khairutdinov, R., *J. Phys. Chem.* **99**, 16646 (1995).
19. Nozik, A. J., *in* "Photocatalytic Purification and Treatment of Water and Air" (D. F. Ollis and H. Al-Ekabi, Eds.), p. 39. Elsevier, Amsterdam, 1993.
20. Linsebigler, A. L., Lu, G., and Yates, J. T., Jr., *Chem. Rev.* **95**, 735 (1995).
21. Almquist C. L. B., Ph.D. dissertation. Aerosol and Air Quality Research Laboratory. University of Cincinnati, 2001.
22. Wang Z. M., Yang, G., Biswas, P., Bresser, W., and Boolchand, P., *Powder Technol.* **114**, 197 (2001).